Surfacing Curve Networks with Normal Control

Tibor Stanko[a,b,c], Stefanie Hahmann[b,c], Georges-Pierre Bonneau[b,c], Nathalie Saguin-Sprynski[a,b]

[a] *CEA, LETI, MINATEC Campus, Grenoble*
[b] *Université Grenoble Alpes*
[c] *CNRS(Laboratoire Jean Kuntzmann), Inria*

Abstract

Recent surface acquisition technologies based on microsensors produce three-space tangential curve data which can be transformed into a network of space curves with surface normals. This paper addresses the problem of surfacing an arbitrary closed 3D curve network with given surface normals. Thanks to the normal vector input, the patch finding problem can be solved unambiguously and an initial piecewise smooth triangle mesh is computed. The input normals are propagated throughout the mesh. Together with the initial mesh, the propagated normals are used to compute mean curvature vectors. We then compute the final mesh as the solution of a new variational optimization method based on the mean curvature vectors. The intuition behind this original approach is to guide the standard Laplacian-based variational methods by the curvature information extracted from the input normals. The normal input increases shape fidelity and allows to achieve globally smooth and visually pleasing shapes.

Keywords: shape reconstruction, curve network, normal input, smooth surface

1. Introduction

Traditionally, digital models of real-life shapes are acquired with 3D scanners, providing point clouds for surface reconstruction algorithms. However, there are situations when 3D scanners fall short, e.g. in hostile environments, for very large or deforming objects. In the last decade, alternative approaches to shape acquisition using data from microsensors have been developed [1, 2]. Small size and cost of these sensors facilitate their integration in numerous manufacturing areas; the sensors are used to obtain information about the equipped material, such as spatial data or deformation behavior. Ribbon-like devices incorporated into soft materials [3] or instrumented mobile devices moving on the surface of an object provide tangential and positional data along geodesic curves – see Figure 2 for an example acquisition setup. In this context, we focus on the resulting problem of surface reconstruction and leave aside all issues related to acquisition and transformation of sensor signals into geometric data.

We address the problem of fitting a smooth surface to given discrete positional and normal data along a network of 3D curves. The goal is to obtain a fully automatic, efficient and robust method producing fair and visual pleasing surfaces consistent with the shape suggested by the input curves. A common practice in shape modeling is to rely on normal vector input in order to enhance shape quality and fidelity. Normal input can be found e.g. as boundary constraints in variational modeling [4, 5, 6], as geometric invariants [7], for computing flowfields guiding the surface construction process, as Hermite data in surface fitting [8, 9] or indirectly describing silhouette constraints [10, 11] or shading behavior of 2D and 3D shapes [12, 13, 14] to cite a few possible applications.

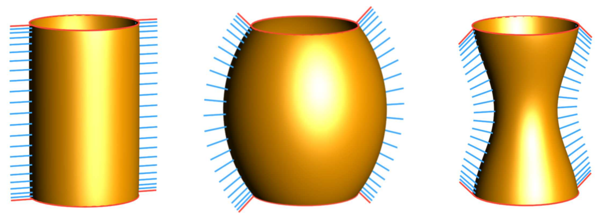

Figure 1: Influence of input normals: the two circular curves (red) are given as input together with normal vectors of different orientation (red normals). Propagation of the input normals over the surface (blue) guides the computation of three different shapes.

More generally, surfacing 3D networks is a fundamental problem in geometric modeling. Apart from traditional CAD modeling [15, 8, 16, 9], sketch-based interfaces [17, 18, 19] and sketch-based modeling techniques [20, 21, 22, 23, 24, 25] have recently become increasingly popular in a range of versatile application areas. Even though normal vectors are not part of a typical sketch-based modeler output [26, 17, 18], recent state of the art [24] in surfacing 3D curve networks however requires estimation of normal vectors along the curve network.

The method we propose is a new mesh-based data-driven variational approach. We show how to generate high quality surfaces faithful to the input data by solving linear systems only. The key insight is the decoupling of normals from positions for the curve-to-patch extrapolation. The method first interpolates positions and normals separately over patches enclosing cycles of curves, then

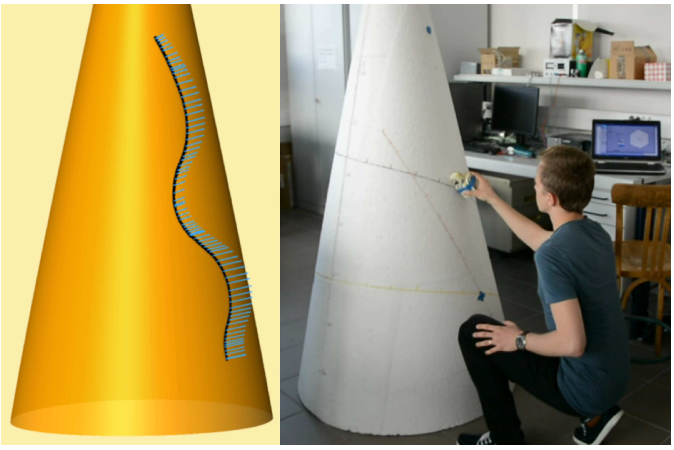

Figure 2: In this example, we scan curves with normals on the cone using the Morphorider, a small mouse-like device instrumented with microsensors. The position and normal information along the scanned curves can serve as input to our algorithm.

estimates mean curvature values at vertices, and finally optimizes for positions that best match the mean curvature vector formed by the mean curvature value and normal computed in the previous steps. The combination of shape and normal optimization into a compact expression has the advantage of not requiring the usual reformulation of normal constraints into layers of positional boundary constraints.

Contributions. This paper is an extended version of the earlier short paper [27] in which we have first introduced a variational approach for smooth surface modeling to fit a given curve network with surface normals. The main contribution of the earlier short paper was to combine the standard Laplacian with a term based on estimation of the mean curvature normal. The intuition behind this original approach was to guide the standard Laplacian-based variational methods by the curvature information extracted from input normals. The normal input increases shape fidelity and allows to achieve globally smooth and visually pleasing shapes.

In comparison with the original short paper, this paper provides an expanded discussion of a modified mean curvature estimation used inside our Laplacian-based surface modeling framework that supports the generation of a continuously varying normal vector field. Our mean curvature estimation blends the positional and normal input so that the solution of our optimization conforms to both constraints. Additionally, we propose a simplified and more compact version of the energy functional used to compute a globally smooth surface with constraints along curve network. Most importantly, we provide more results, a convergence analysis and an in-depth comparison of our algorithm with state of the art methods.

2. Related work

Surfacing curve networks. With the advent of sketch-based modeling tools, such as interactive 3D sketching tools [26, 28, 17, 18] or methods inferring 3D curve networks from 2D sketches [29, 19], considerable effort has been dedicated to the design of methods for surfacing curve networks originating from sketching tools [20, 30, 31, 32, 24]. The common assumption in these works is that the underlying curve network was created with some design intent, and that the input information is minimal. Rose et al. [20] solve the patch finding problem and compute a developable boundary triangulation. Bessmeltsev et al. [31] interpolate a general 3D network of curve cycles by computing quad-mesh patches whose isolines capture the design flow inherent in the network. Sadri and Singh [32] compute self-intersection-free surface patches based on a flow complex induced by the boundary curves. Both methods compute surface patches individually and do not seek a globally smooth surface across dedicated boundary curves as we do. Pan et al. [24] use rotation-minimizing frames along the curves to estimate normal vector input and construct globally smooth surface patches having a curvature direction field consistent with an orthogonal flow field implied by the boundary curves. This makes sense in the setting of sketch-based modeling where the artist-drawn input represents particular characteristic shape curves, such as representative flow-lines. This is a strong assumption on the input network we do not make; our input curves, in contrast, can have arbitrary shapes (Figure 9).

n-sided patches. n-sided boundary patches – possibly with prescribed tangent ribbons to achieve G^1-continuity across boundary curves – can be computed using transfinite interpolation methods (Coons patches [15], Gregory patches [8], Generalized Bézier patches [9] or subdivision approaches [33]). The first group of methods assumes a pre-segmentation of each input cycle into n curve segments with low-distortion mapping to a convex planar n-sided polygon. Prescribed tangent ribbons must be defined consistently and twists estimated accordingly. Methods in the second group quadrangulate the input cycles with topological guarantees on the extraordinary vertices and approximate the coarse mesh using well-known subdivision schemes. The variational approach of Boier-Martin et al. [34] integrates normal constraints by locally fitting the vertex neighborhood with a quadratic polynomial in order to estimate partial derivatives. However, the integration of normal constraints violates the independence of spatial dimensions of the linear system to solve.

Shading-based variational modeling. Gingold and Zorin [12] modify a given input shape by drawing strokes on a shaded image of the surface. The strokes indirectly impose normal constraints that are solved by modifying the position of the surface along the strokes, while the normals of the surface outside the strokes should not change. In contrast, we impose both positional and normal constraints along input curves, and compute new positions and normals everywhere else.

Variational modeling with normal constraints. The minimum variation surfaces [35] enable direct prescription of normals and principal curvatures along a curve network and may result in high quality shapes; however, the resulting optimization is nonlinear. Thanks to their speed and robustness, linear variational surface modeling and deformation methods have attracted an impressive amount of interest in the past few years, even though they only provide approximate results with respect to nonlinear problems; see the survey by Botsch and Sorkine [36]. We focus on linear methods using normal constraints in addition to standard positional constraints. The boundary constraint modeling methods of Botsch and Kobbelt [4], Jacobson et al. [5], and Andrews et al. [6] prescribe C^k continuity indirectly either by fixing $k-1$ rings of vertices or by adding a ghost geometry. Setting additional rings of vertices consistently with C^k continuity at intersections of constrained curves is not a trivial task. This issue, referred to as twist compatibility problem or vertex consistency problem [37], arises when joining smooth patches around a common vertex of arbitrary valence with tangent plane continuity. Jacobson et al. [5] solve the problem by freezing the 1-neighborhood of each vertex with normal constraint. Vertices with conflicting neighborhoods are fixed in the least-squares sense. Andrews et al. [6] propose a linear variational modeling system from curve networks using a ghost geometry for solving inconsistent Laplacian constraints. This technique only enables to generate sharp edges along arbitrary curves. Schneider and Kobbelt [38] propose a multigrid fairing method with prescribed positions and normals; only constraints along simple curves are considered. Crane et al. [39] present a fairing method using Willmore flow expressed in curvature space that allows to prescribe positions and binormal vectors along the surface boundary.

All these methods share the treatment of normals as boundary constraints when computing the positions. Our approach is different. By separately interpolating normals and positions before combing them into a mean curvature vector field which is then used to compute the best matching surface, the propagated normals serve as a guiding vector field as illustrated in Figure 1. We therefore avoid the vertex consistency problem and can deal with normal constraints even at the intersection of multiple curves. More importantly, unlike all the approaches above, our method does not require an extra parameter to control the magnitude of normals.

3. Framework

The surface $\mathcal{S}$ we aim to reconstruct is a connected 2-manifold, with or without boundary, parameterized by $\mathbf{p} : \Omega \subset \mathbb{R}^2 \to \mathcal{S} \subset \mathbb{R}^3$. Moreover, the tangent space $T_{\mathbf{p}}(\mathcal{S})$ varies continuously. Next, we consider a curve network $C \subset \mathcal{S}$ which is connected and closed. The curves $\mathbf{c}_k(t) = \mathbf{p}(u(t), v(t)) \in C$ are C^1 smooth and without self-intersections; the intersection of two different curves is either empty or a discrete set of points. Knowing the topology of the curve network C, the input to our algorithm is a discrete sample of positions $\mathbf{p}_i = \mathbf{c}_k(t_i) = \mathbf{p}(u(t_i), v(t_i)) \in C$, together with the unit surface normals $\mathbf{n}_i \perp T_{\mathbf{p}_i}(\mathcal{S})$.

3.1. Overview of the method

We use the following pipeline to generate a globally smooth surface from curve and normal vector input:

1. Raw data are first interpolated with cubic splines and resampled uniformly. We efficiently detect the network cycles, then triangulate them in plane.
2. By solving two biharmonic systems with boundary constraints, we both propagate the surface normals and obtain an initial guess for the vertex positions; this allows us to compute discrete mean curvature for the whole mesh.
3. Finally, we solve a linear optimization problem computing a surface that best matches the mean curvature vector formed by the mean curvature value and the normal computed in the previous step.

3.2. Exploiting local tangent space to detect cycles

The detection of cycles in a general curve network is a complex and ambiguous problem, often without a unique solution. In order to overcome this problem, methods for surfacing sketched networks adopt a variety of heuristics to mimic the human perception [30]. In our specific setting, due to the assumptions on surface smoothness and manifoldness, and the availability of the oriented normals, any possible ambiguity can be efficiently resolved as follows.

Let us call a *node* the intersection between two or more curves. A *segment* is a portion of curve bounded by two adjacent nodes. A *cycle* is a set of adjacent segments which constitute a boundary of some surface patch; the curve cycles are assumed to be contractible on $\mathcal{S}$. Our algorithm is inspired by face extraction in edge-based data structures for manifolds. First, the segments adjacent to any node are cyclically sorted with respect to the orientation given by the input normal at that node. Then, starting from any (Node, Segment) pair, we trace a unique cycle by choosing the next node as the other endpoint of the current segment. The next segment is then picked from the ordered set. To handle surfaces with boundary, we require the user to tag all boundary segments.

3.3. Network tessellation

We represent the surface $\mathcal{S}$ as a triangle mesh $\mathcal{M} = (\mathcal{V}, \mathcal{F})$ with vertices $\mathcal{V}$ and faces $\mathcal{F}$. Prior to the tessellation, the positions $\mathbf{p}_i$ and normals $\mathbf{n}_i$ along the curve network C are interpolated with cubic splines and resampled with arc length parameterization, providing a uniformly sampled network (Figure 8 top). Each cycle defines a closed 3D curve Γ bounding an n-sided surface patch. We triangulate a planar projection of each cycle individually to obtain the topology $\mathcal{F}$ of the whole mesh; the triangulation is computed using Shewchuk's Triangle [40]. The plane of projection for each cycle is defined by the average position $\tilde{\mathbf{p}}$ and average unit normal $\tilde{\mathbf{n}}$ computed from resampled Γ.

Even though this simple planar projection is not necessarily injective, we have found that it leads to a much smaller distortion between the planar triangulation and the mesh triangulation, in comparison with other planar embeddings of Γ with guaranteed injectivity (e.g. mapping to a circle or a polygon). Notice that a more robust but time-consuming 3D curve tessellation method can be used [41].

3.4. Variational smoothing

At this point of the process we have computed the topology $\mathcal{F}$ of the mesh $\mathcal{M}$, and we have the constraints – positions and normals – for vertices along the resampled curve network C. In this section, we describe a variational method for computing the positions of the free vertices, based on the discretization of the Laplace-Beltrami operator and of the mean curvature vector for piecewise linear surfaces.

Discretization of Δ. Given a piecewise-linear function $f_i = f(\mathbf{v}_i)$ defined over the vertices $\mathbf{v}_i \in \mathcal{V}$ of $\mathcal{M}$, the discretization of the Laplace-Beltrami has the form [36]

$$\Delta f(\mathbf{v}_i) = w_i \sum_{j \in N_1(i)} w_{ij}(f_j - f_i)$$

where $N_1(i)$ is the index set of 1-ring neighborhood of $\mathbf{v}_i$. The vertex weights are stored in the diagonal mass matrix $\mathbf{M}_{ii} = 1/w_i$, while the edge weights w_{ij} are stored in a symmetric matrix $\mathbf{L}_s$

$$(\mathbf{L}_s)_{ij} = \begin{cases} -\sum_{k \in N_1(i)} w_{ik}, & i = j, \\ w_{ij}, & j \in N_1(i), \\ 0, & \text{otherwise.} \end{cases}$$

The discrete Laplace operator is then characterized by the matrix $\mathbf{L} = \mathbf{M}^{-1}\mathbf{L}_s$. In the following, we use the cotangent Laplacian $w_i = 1/A_i, w_{ij} = \frac{1}{2}(\cot\alpha_{ij} + \cot\beta_{ij})$ where α_{ij} and β_{ij} are the two angles opposite to the edge (i, j), and A_i is the Voronoi area of $\mathbf{v}_i$ [42].

Initial vertices and propagated normals. Let $\mathcal{V}_c$ denote the set of vertices lying on the curve network C, and $\mathcal{V}_f$ denote the remaining free vertices. We start by computing initial positions and initial normals for all vertices by solving two biharmonic systems: $\mathbf{L}^2\mathbf{V}^* = \mathbf{0}$ for positions and $\mathbf{L}^2\mathbf{N}^* = \mathbf{0}$ for normals. The *propagated normals* $\mathbf{N}^*$ are then normalized. We choose $\mathbf{L}$ as the cotangent Laplacian based on the planar triangulation computed in Section 3.3. The positional and normal boundary conditions are incorporated into the systems as hard constraints by eliminating the corresponding rows of the matrix $\mathbf{L}^2$ as described in [43].

Mean curvature guide. From the initial vertices $\mathbf{v}^*$ and the propagated normals $\mathbf{n}^*$ we now compute mean curvature information that will guide the optimization. Following Sullivan [44], the discrete mean curvature vector at a mesh vertex $\mathbf{v}$ is proportional to the integral of the conormal $\eta = \mathbf{n} \times \mathbf{e}$, i.e. the vector product of the normal and the unit tangent to the boundary,

$$2\mathbf{h}(\mathbf{v}) = \oint_{\partial N_1} \eta \, ds$$

computed along the boundary of the 1-neighborhood N_1 of $\mathbf{v}$. Sullivan [44] evaluates this integral using the triangle normals defined by the mesh vertices $\mathbf{v}$.

In order to take the input data into account, we evaluate this integral using the propagated normals $\mathbf{n}^*$ rather than the triangle normals. More precisely, we compute the mean curvature vector for the initial surface by summing the contributions for all oriented edges opposite to $\mathbf{v}^*$:

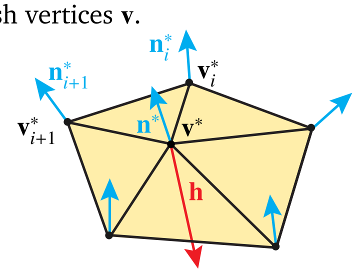

$$\mathbf{h}(\mathbf{v}^*) = \frac{1}{A} \sum_{i=0}^{n-1} \frac{\mathbf{n}^* + \mathbf{n}^*_i + \mathbf{n}^*_{i+1}}{\|\mathbf{n}^* + \mathbf{n}^*_i + \mathbf{n}^*_{i+1}\|} \times (\mathbf{v}^*_{i+1} - \mathbf{v}^*_i), \qquad (1)$$

where $\mathbf{n}^*$ denotes the propagated normal at the vertex $\mathbf{v}^*$ of valence n, whose Voronoi area is A and its neighbors are $\mathbf{v}^*_i$ (indices taken modulo n, see inset).

Formula (1) for computing the mean curvature is a key part to our method. Its originality lies in blending together the positional information (the initial vertices $\mathbf{v}^*$) with the additional normal information (the propagated normals $\mathbf{n}^*$) not directly inferred from the positions. In contrast, the usual discrete mean curvature formulations, such as the cotan formula [42], rely solely on vertex positions. We illustrate this originality in Figure 3, where we show three discrete mean curvatures, one based on [42] (left), and two on our formula (1) (middle and right) computed with the same geometry, but using two different normal fields. It can further be observed in Figure 3 that our mean curvature measure behaves at least as well as the standard measures even with a low quality mesh. Since we apply the mean curvature formula in this paper to good quality triangulations resulting from a planar Delaunay tessellation (Section 3.3) we did not investigate the incorporation of propagated normals into more robust discrete mean curvature measures such as [45].

Figure 3: Mean curvature of the irregular horse mesh. (Left) the cotan formula [42] which is based solely on the mesh vertices, (middle & right) the 3-averaging formula (1), which additionally takes into account a normal at each vertex. For the middle image, the vertex normal is taken as the average of the face normals. In the rightmost example we smoothed the vertex normals before applying formula (1).

Optimization. We can now define the energy functional

$$E(\mathcal{V}) = \sum_{\mathbf{v}\in\mathcal{V}} ||\Delta\mathbf{v} + h(\mathbf{v})\mathbf{n}^*||^2 \tag{2}$$

with $h(\mathbf{v}) = ||\mathbf{h}(\mathbf{v})||$ being the scalar mean curvature at $\mathbf{v}$. This formulation, derived from the well-known formula $\Delta\mathbf{v} = -h\,\mathbf{n}$, enables us to match the mean curvature and the propagated normals. In order to exactly interpolate the positional constraints $\mathcal{V}_c$, we perform the following optimization:

$$\min E(\mathcal{V}) \quad \text{s.t.} \quad \mathbf{v} = \mathbf{v}^* \text{ for all } \mathbf{v}\in\mathcal{V}_c\,. \tag{3}$$

The energy E is written in matrix form as

$$E(\mathcal{V}) = ||\mathbf{L}\mathbf{V} - 2\mathbf{H}||^2$$

and minimized by solving

$$\begin{bmatrix}\mathbf{L}^\top\mathbf{L} & \mathbf{C}^\top\\ \mathbf{C} & \mathbf{0}\end{bmatrix}\begin{bmatrix}\mathbf{V}\\ \Lambda\end{bmatrix} = \begin{bmatrix}\mathbf{L}^\top\mathbf{H}\\ \mathbf{V}_c^*\end{bmatrix}$$

with

$$\mathbf{C} = \begin{bmatrix}\mathbf{I}_c & \mathbf{0}\end{bmatrix}, \quad \mathbf{V} = \begin{bmatrix}\mathbf{V}_c\\ \mathbf{V}_f\end{bmatrix},$$

where Λ is the matrix of Lagrange multipliers, $\mathbf{I}_c$ is the $c\times c$ identity matrix, and $\mathbf{H}$ is the matrix of propagated normals $\mathbf{N}^*$ scaled by the mean curvature h.

4. Results

4.1. Normal control

In Figure 1 we demonstrate the shape control provided by the input normals. The fixed vertex positions are sampled along two parallel circles from the same cylinder while prescribing three different sets of normal vectors along the circles. With the original normals (Fig. 1 left), the cylindrical surface is nicely reconstructed. Using the two other sets of rotated normals (Fig. 1 middle, right) results in the barrel and bottleneck surfaces, as expected intuitively. The method works well even for challenging input data, such as the networks with large normal curvature variations and high valence curve intersections in Figure 8, or networks with large curvature variation in the tangent plane in Figure 9.

4.2. Comparison with previous methods

Botsch and Kobbelt [4] state that solving for the k^{th}-order Laplacian while imposing boundary conditions up to C^{k-1} implies a non-trivial smooth solution:

$$\begin{aligned}\Delta^k S(x) &= 0, && x\in\Omega\backslash\delta\Omega;\\ \Delta^j S(x) &= b_j(x), && x\in\delta\Omega,\ j<k.\end{aligned} \tag{4}$$

Notice that the authors in [4] did not implement boundary constraints directly; instead, they fixed positions of $k-1$ rings of vertices to prescribe C^{k-1} boundary constraints. This setting prevents dealing with arbitrary constrained curve networks without knowing the positions of $k-1$ rings of vertices. It is therefore impossible to compare our method to theirs; we can however compare our method to the analogous formulation given by (4). To this end, we have implemented the system (4) for $k = 2$. To avoid fixing the positions of 1-ring vertices along constrained curves, we directly cast the b_1 as equality constraints of the linear system. See Figure 5 for visual comparison of various error metrics on sphere and torus, and Table 1 for numerical analysis of distance to ground truth.

The method of Pan et al. [24] is considered the state of the art in surfacing sketched curves. We find it interesting to include a comparison with this method, although the two algorithms do not share the same input since [24] do not know the normals a priori. The comparison with their method on the gamepad is shown in Figure 4. The normals along the constrained curves, required by our method, were sampled from the final surface of Pan et al. [24]. From left to right, we show the output of Pan et al. [24], the surface computed with constrained linear differential equation method (4) with direct prescription of normals, and our surface.

Our method combines the algorithmic simplicity with high fidelity to the reconstructed shape, and at the same time maintains the fairness of the final surface. Interesting details are revealed by looking at the isophotes. On the surface of Pan et al. [24], the isophotes are of globally poor quality, with undesirable wiggles visible at closer inspection, see the close-up to the concave region.

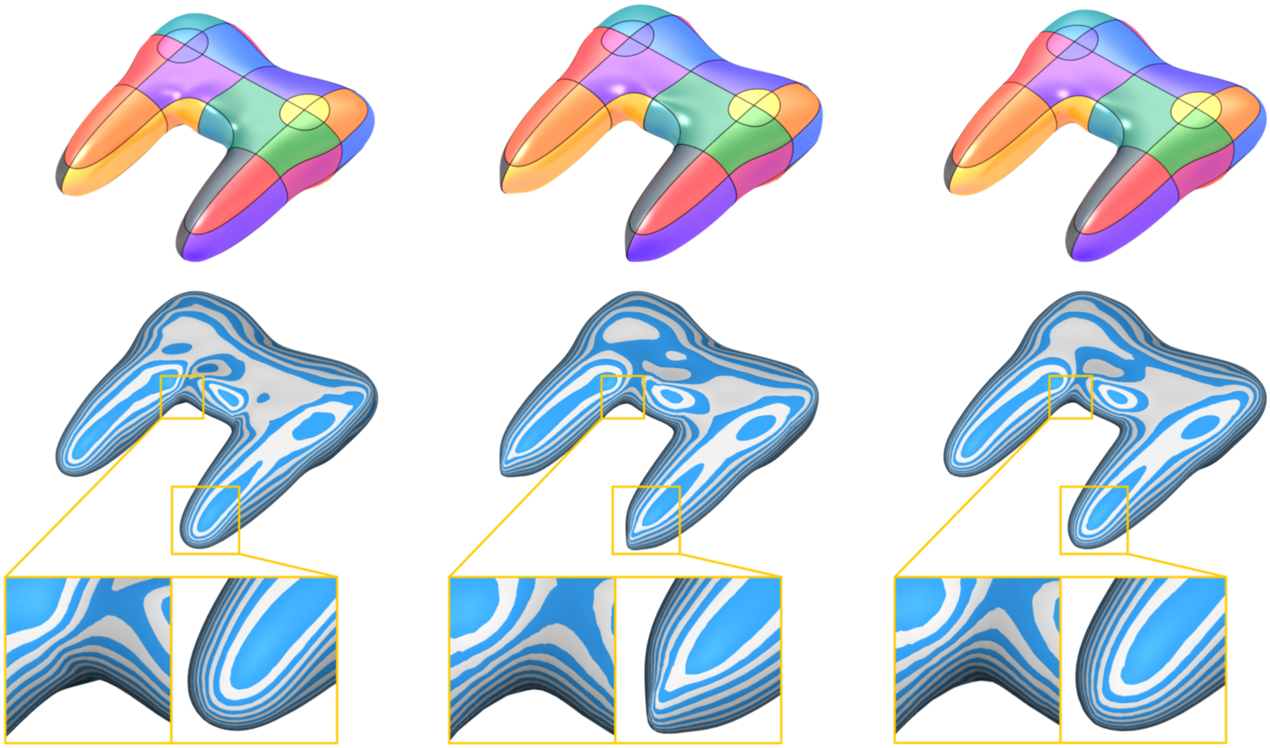

Figure 4: On sketched networks, the results of our algorithm are similar to the method of Pan et al. [24], which assumes the input curves capture the flow field of the underlying surface. The isophotes on our surface vary more smoothly, suggesting higher order of continuity. Left to right: the method of Pan et al. [24]; the formulation (4) (Section 4.2) with direct prescription of normals; our algorithm. All three meshes have the same normals along the curve network.

While the middle surface computed with (4) seems globally smoother than the left surface, the linearization artifacts are evident (close-up, handle). The colored renderings of the three surfaces look similar at the first glance; notice however the improved quality of specular highlights on our gamepad compared to the left surface.

4.3. *Measuring the error*

In Figure 5 we compare three error measures on well known geometries, the sphere and the torus: mean curvature, distance to ground truth and difference between propagated and computed normals. We compare the error from the standard biharmonic and triharmonic surfaces with positional constraints along the curve network (left two columns) and the method (4) (middle right) with our surfaces (right column). We also show the isophote pattern which indicates globally smooth shapes, also across the curve network.

Notice that the standard linear variational methods exhibit the well-known undesired defects due to the linearization of the energy functionals, and the shapes have high curvatures along the curve network and low curvature everywhere else. In contrast our solution has a much smaller curvature variation. Many authors spend considerable effort in improving the shape of linear methods using e.g. reparameterizations or multigrid methods [38, 4, 5]. It can be observed that our shapes succeed in mimicking the

data	method	# $\mathcal{V}_f$ / $\mathcal{V}_c$	distance error ($\mathcal{V}_f$ only)			
			min	max	mean	RMS
sphere, $r = 1$	ours	19545 / 738	0.0004	0.0502	0.0319	0.0343
	method (4)		0.0001	0.3262	0.1412	0.1635
	biharmonic		0.0006	0.2887	0.1465	0.1669
	triharmonic		0.0003	0.3994	0.1641	0.1918
torus, $R = 4, r = 2$	ours	24321 / 564	0.0008	0.3207	0.1260	0.1464
	method (4)		0.0021	0.7917	0.4095	0.4587
	biharmonic		0.0028	0.7967	0.4122	0.4624
	triharmonic		0.0016	0.6068	0.3255	0.3626

Table 1: Distance from analytic ground truth, measured on the free vertices.

desired non-linear shape behaviors simply by combining two linear processing steps: normal propagation and constrained fitting, see the curvature plots in Figure 5. We argue that the normal propagation step which precomputes a continuously varying normal field is a key ingredient for this nice property.

4.4. *Convergence analysis*

Given an input curve network, we have computed a sequence of initial planar triangulations (Section 3.3) with a sampling distance divided by two, resulting in a number of triangles approximately multiplied by four. We then applied our variational smoothing method (Section 3.4). This process results in a sequence of meshes $\mathcal{M}_i$. Since there is no analytic form of $\lim_{i\to\infty} \mathcal{M}_i$, we illustrate the

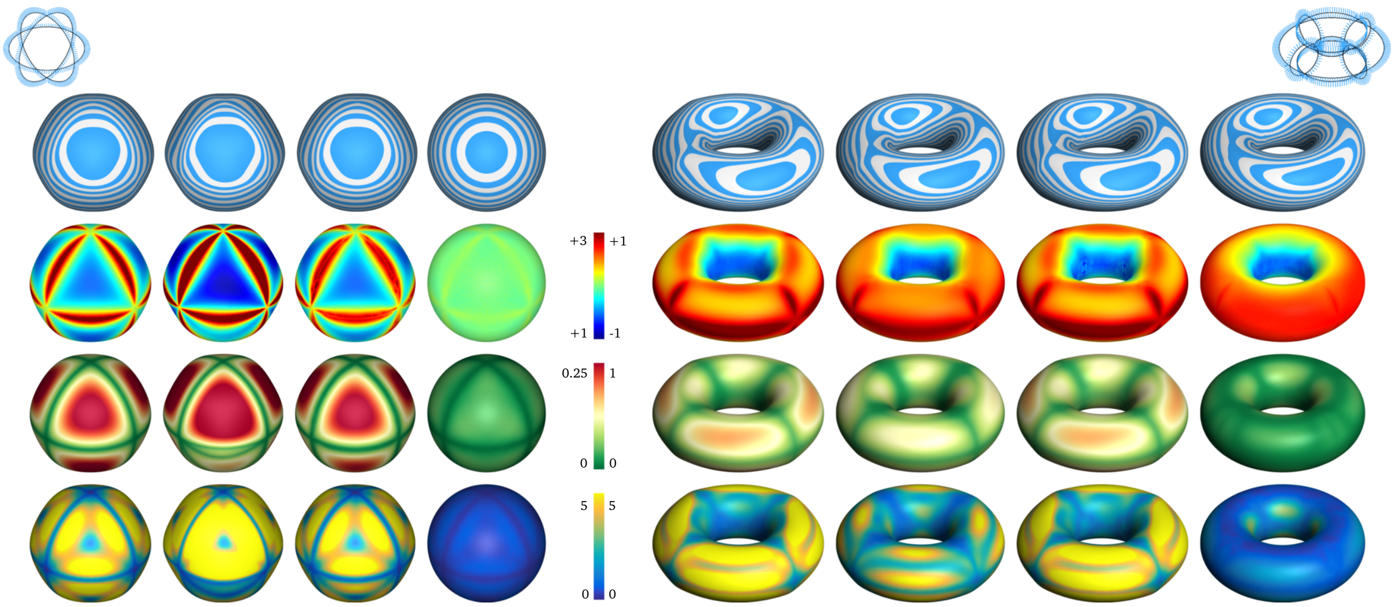

Figure 5: Various error measures on the unit sphere and the torus with radii 4 and 2. Top to bottom: isophotes, mean curvature, distance from ground truth (Table 1), difference between propagated and computed normals (in degrees). Left to right: biharmonic surface $\Delta^2 = \mathbf{0}$, triharmonic surface $\Delta^3 = \mathbf{0}$, method (4), our algorithm.

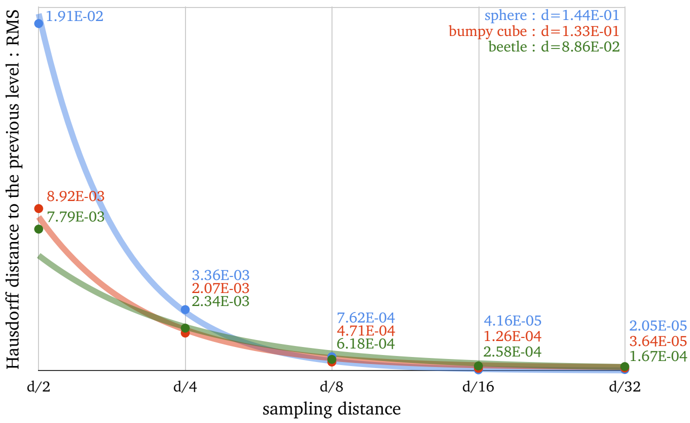

Figure 6: The meshes computed using our method converge towards a limit surface upon refinement of the sampling distance; see Section 4.4 for details.

convergence in Figure 6 by plotting the Hausdorff distance between the consecutive meshes $\mathcal{M}_i, \mathcal{M}_{i+1}$. The three curves correspond to the sphere (Fig. 5), the beetle and the bumpy cube (Fig. 8) networks.

4.5. Hard constraints vs. soft constraints

Until now, in all of our examples, the positions of all vertices along input curves were exactly interpolated as hard constraints by solving (3). In case of noisy input data, which usually occurs when acquiring data with scanning or mobile devices (see Section 1), it might be useful to modify the problem (3) in order to incorporate soft positional constraints as follows:

$$E_{soft}(\mathcal{V}) = \sum_{\mathbf{v}\in\mathcal{V}} \|\Delta\mathbf{v} + 2h(\mathbf{v})\mathbf{n}^*\|^2 + \omega \sum_{\mathbf{v}_s\in\mathcal{V}_s} \|\mathbf{v}_s - \mathbf{v}_s^*\|^2$$

where the constrained vertices $\mathcal{V}_c$ are further partitioned into hard constraints $\mathcal{V}_h$ and soft constraints $\mathcal{V}_s$. Figure 7 illustrates the robustness of this approach; in this test, we artificially perturbed the positions and normal directions along the input network. Our method with soft constraints produces stable output, while still preserving the shape fidelity.

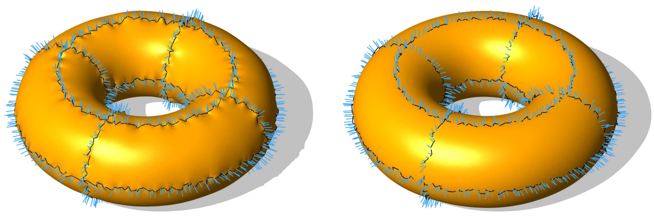

Figure 7: If the input data are noisy, soft constraints (right) produce better results than hard constraints (left) while still maintaining high overall shape fidelity. In this example, we artificially added 5% of noise to both positions and normals.

5. Limitations

A weakness of our method lies in the fact that the cotangent weights for the Laplacian matrix $\mathbf{L}$ are inferred from the planar triangulation, computed for each patch individually as explained in Section 3.4. Such parametrization is not isometric to the actual surface patch; as a consequence, the weights are not optimal. Nevertheless our examples show that it does not impact the smoothness of our results across surface patches.

The framework cannot automatically handle curve networks which are open or consist of more than one component. However, the optimization (3) is not limited by the

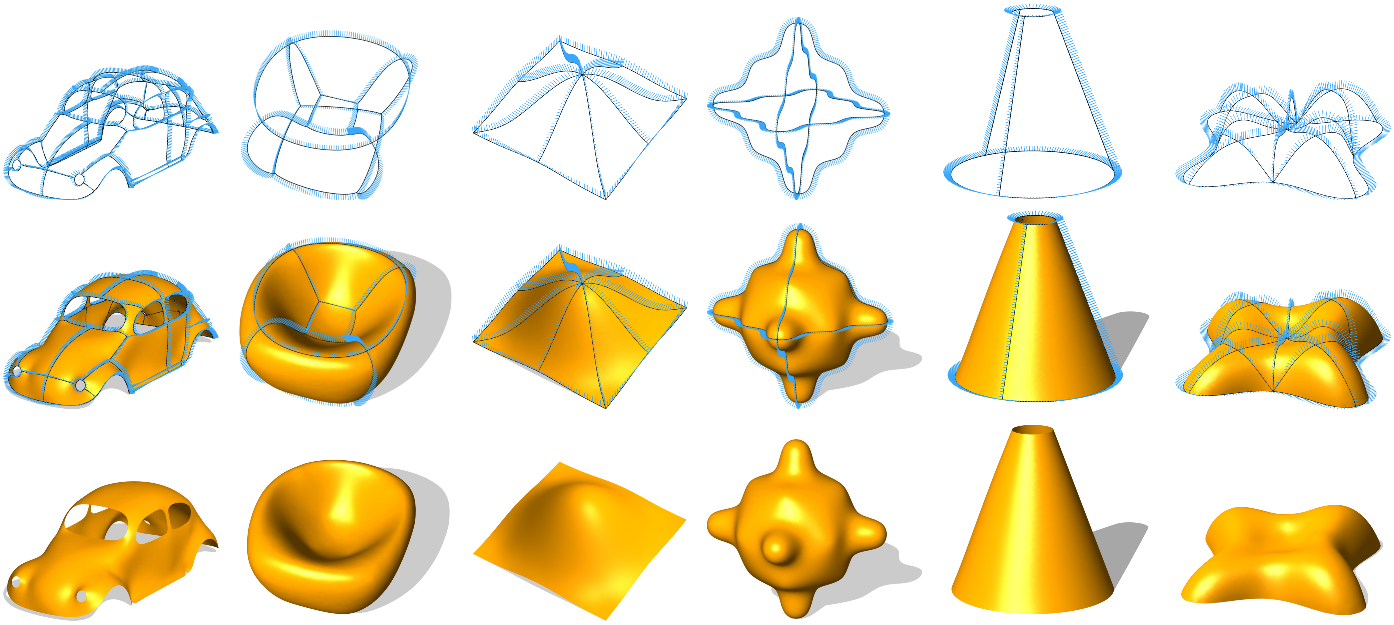

Figure 8: Smooth surfaces reconstructed using our method.

topology of the network, only by the availability of the initial mesh.

6. Conclusion

We have introduced a Laplacian-based surface reconstruction method from curve and normal input. After propagating the input normals smoothly over the surface and computing the corresponding mean curvature vectors, the normal constraints are integrated into the energy functional. Efficiency and robustness are achieved by using a linearized objective functional, such that the global optimization amounts to solving a sparse linear system of equations.

The presented framework is intended to serve for curve networks with normal vectors acquired by mobile devices equipped with microsensors. For this application we plan the following extensions. The method, currently requiring a closed curve network, could be modified to work with open curve networks. The initial tessellation could be improved by using a more advanced 3D patching algorithm. Since our current implementation runs at interactive time rates (order of 0.1s for a mesh with 10k vertices and 1k constraints), we plan to allow the user to scan shapes interactively by incrementally adding curves. We therefore want to investigate how to update the optimization when the input data changes locally.

Acknowledgment. The meshes used in our tests were kindly provided by Pan et al. [24] (gamepad), Leif Kobbelt (beetle), Cindy Grimm[1] (bowl), and libigl[2] (lilium, bumpy cube).

[1] http://web.engr.oregonstate.edu/~grimmc/
[2] http://libigl.github.io/libigl/

References

[1] Sprynski N, David D, Lacolle B, Biard L. Curve Reconstruction via a Ribbon of Sensors. In: 14th IEEE Int. Conf. on Electronics, Circuits and Systems. 2007, p. 407–10.
[2] Hoshi T, Shinoda H. 3D Shape Measuring Sheet Utilizing Gravitational and Geomagnetic Fields. In: SICE Annual Conf. 2008, p. 915–20.
[3] Saguin-Sprynski N, Jouanet L, Lacolle B, Biard L. Surfaces Reconstruction Via Inertial Sensors for Monitoring. In: 7th European Workshop on Structural Health Monitoring. 2014, p. 702–9.
[4] Botsch M, Kobbelt L. An Intuitive Framework for Real-time Freeform Modeling. ACM Trans Graph (Proc SIGGRAPH) 2004;23(3):630–4.
[5] Jacobson A, Tosun E, Sorkine O, Zorin D. Mixed Finite Elements for Variational Surface Modeling. Computer Graphics Forum (Proc SGP) 2010;29(5):1565–74.
[6] Andrews J, Joshi P, Carr N. A Linear Variational System for Modelling From Curves. Computer Graph Forum 2011;30(6):1850–61.
[7] Huard M, Sprynski N, Szafran N, Biard L. Reconstruction of Quasi Developable Surfaces from Ribbon Curves. Numerical Algorithms 2013;63(3):483–506.
[8] Gregory JA, Zhou J. Filling Polygonal Holes with Bicubic Patches. Computer Aided Geometric Design 1994;11(4):391 – 410.
[9] Várady T, Salvi P, Karikó G. A Multi-sided Bézier Patch with a Simple Control Structure. CGF 2016;35(2):307–17.
[10] Igarashi T, Matsuoka S, Tanaka H. Teddy: A Sketching Interface for 3D Freeform Design. In: Proceedings of SIGGRAPH 99, Annual Conference Series. New York, NY, USA: ACM Press/Addison-Wesley Publishing Co. ISBN 0-201-48560-5; 1999, p. 409–16.
[11] Nealen A, Sorkine O, Alexa M, Cohen-Or D. A Sketch-based Interface for Detail-preserving Mesh Editing. ACM Trans Graph (Proc SIGGRAPH) 2005;24(3):1142–7.
[12] Gingold Y, Zorin D. Shading-based Surface Editing. ACM Trans Graph (Proc SIGGRAPH) 2008;27(3):1–9.
[13] Sýkora D, Kavan L, Čadík M, Jamriška O, Jacobson A, Whited B, et al. Ink-and-ray: Bas-relief Meshes for Adding Global Illumination Effects to Hand-drawn Characters. ACM Trans Graph (Proc SIGGRAPH) 2014;33(2):16:1–16:15.
[14] Iarussi E, Bommes D, Bousseau A. Bendfields: Regularized Curvature Fields from Rough Concept Sketches. ACM Trans Graph (Proc SIGGRAPH) 2015;34(3):24.
[15] Farin G. Curves and Surfaces for CAGD: A Practical Guide. 5th ed.;

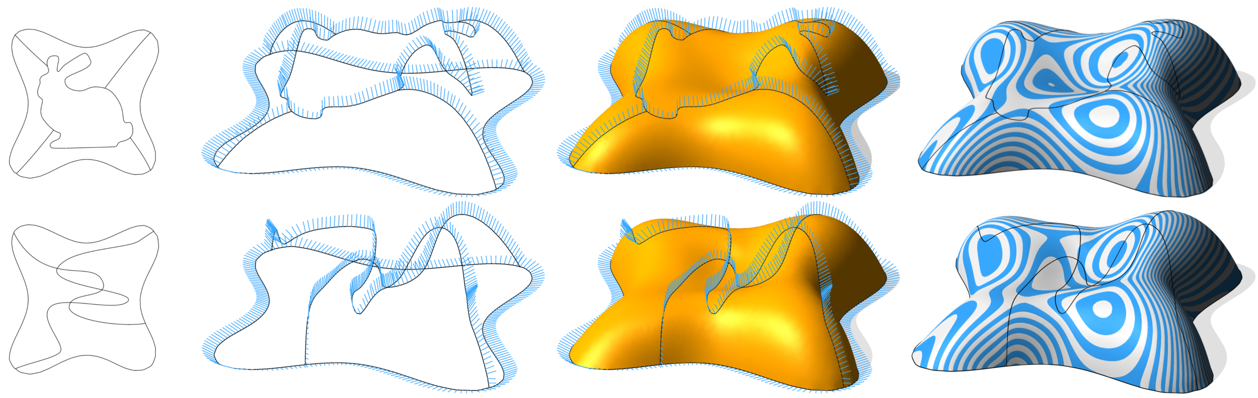

Figure 9: In terms of geometry, we place no constraints on the input. Our method can handle even these challenging networks with winding curves, all while preserving the global smoothness across patches.

San Francisco, CA, USA: Morgan Kaufmann Publishers Inc.; 2002. ISBN 1-55860-737-4.

[16] Farin G, Hansford D. Discrete Coons Patches. Computer Aided Geometric Design 1999;16(7):691 – 700.

[17] Bae SH, Balakrishnan R, Singh K. ILoveSketch: As-Natural-As-Possible Sketching System for Creating 3D Curve Models. In: UIST 08. ACM; 2008, p. 151–60.

[18] Schmidt R, Khan A, Singh K, Kurtenbach G. Analytic Drawing of 3D Scaffolds. ACM Trans Graph (Proc SIGGRAPH Asia) 2009;28(5):149:1–149:10.

[19] Xu B, Chang W, Sheffer A, Bousseau A, McCrae J, Singh K. True2Form: 3D Curve Networks from 2D Sketches via Selective Regularization. ACM Trans Graph (Proc SIGGRAPH) 2014;33(4):131:1–131:13.

[20] Rose K, Sheffer A, Wither J, Cani MP, Thibert B. Developable Surfaces from Arbitrary Sketched Boundaries. In: Proc. Symp. Geom. Proc. 2007, p. 163–72.

[21] Rivers A, Durand F, Igarashi T. 3D Modeling with Silhouettes. ACM Trans Graph (Proc SIGGRAPH) 2010;29(4):1–8.

[22] Umetani N, Kaufman DM, Igarashi T, Grinspun E. Sensitive Couture for Interactive Garment Modeling and Editing. ACM Trans Graph (Proc SIGGRAPH) 2011;30(4):90:1–90:12.

[23] Tasse FP, Emilien A, Cani MP, Hahmann S, Dodgson N. Feature-Based Terrain Editing from Complex Sketches. Computers & Graphics 2014;45:101 –15.

[24] Pan H, Liu Y, Sheffer A, Vining N, Li CJ, Wang W. Flow-Aligned Surfacing of Curve Networks. ACM Trans Graph (Proc SIGGRAPH) 2015;34(4):127:1–127:10.

[25] Jung A, Hahmann S, Rohmer D, Begault A, Boissieux L, Cani MP. Sketching Folds: Developable Surfaces from Non-Planar Silhouettes. ACM Trans Graph 2015;34(5):155:1–155:12.

[26] Nealen A, Igarashi T, Sorkine O, Alexa M. FiberMesh: Designing Freeform Surfaces with 3D Curves. ACM Trans Graph (Proc SIGGRAPH) 2007;26(3).

[27] Stanko T, Hahmann S, Bonneau GP, Saguin-Sprynski N. Smooth interpolation of curve networks with surface normals. In: Bashford-Rogers T, Santos LP, editors. EG 2016 – Short Papers. Lisbon, Portugal: Eurographics Association; 2016, p. 21 –4.

[28] Kara LB, Shimada K. Sketch-Based 3D-Shape Creation for Industrial Styling Design. IEEE Computer Graphics and Applications 2007;27(1):60–71.

[29] Das K, Diaz-Gutierrez P, Gopi M. Sketching FreeForm Surfaces Using Network of Curves. In: Jorge J, Igarashi T, editors. Eurographics Workshop on Sketch-Based Interfaces and Modeling. 2005,.

[30] Zhuang Y, Zou M, Carr N, Ju T. A General and Efficient Method for Finding Cycles in 3D Curve Networks. ACM Trans Graph (Proc SIGGRAPH Asia) 2013;32(6):180:1–180:10.

[31] Bessmeltsev M, Wang C, Sheffer A, Singh K. Design-driven Quadrangulation of Closed 3D Curves. ACM Trans Graph (Proc SIGGRAPH Asia) 2012;31(6):178:1–178:11.

[32] Sadri B, Singh K. Flow-complex-based Shape Reconstruction from 3D Curves. ACM Trans Graph 2014;33(2):20:1–20:15.

[33] Schaefer S, Warren J, Zorin D. Lofting Curve Networks Using Subdivision Surfaces. In: Proc. Symp. Geom. Proc. 2004, p. 103–14.

[34] Boier-Martin I, Ronfard R, Bernardini F. Detail-preserving Variational Surface Design with Multiresolution Constraints. In: Proc. Shape Modeling Applications. 2004, p. 119–28.

[35] Moreton HP, Séquin CH. Functional Optimization for Fair Surface Design. Computer Graphics (SIGGRAPH) 1992;26(2):167–76.

[36] Botsch M, Sorkine O. On Linear Variational Surface Deformation Methods. IEEE Trans Vis Comput Graphics 2008;14(1):213–30.

[37] Farin G. A Construction for Visual C1 Continuity of Polynomial Surface Patches. Computer Graphics and Image Processing 1982;20(7):272–82.

[38] Schneider R, Kobbelt L. Geometric Fairing of Irregular Meshes for FreeForm Surface Design. Computer Aided Geometric Design 2001;18(4):359–79.

[39] Crane K, Pinkall U, Schröder P. Robust Fairing via Conformal Curvature Flow. ACM Trans Graph (Proc SIGGRAPH) 2013;32.

[40] Shewchuk JR. Triangle: Engineering a 2D Quality Mesh Generator and Delaunay Triangulator. In: Applied computational geometry towards geometric engineering. Springer; 1996, p. 203–22.

[41] Zou M, Ju T, Carr N. An Algorithm for Triangulating Multiple 3D Polygons. Computer Graphics Forum (SGP) 2013;32(5):157–66.

[42] Meyer M, Desbrun M, Schröder P, Barr AH. Discrete Differential Geometry Operators for Triangulated 2-manifolds. In: Visualization and mathematics III. Springer; 2003, p. 35–57.

[43] Botsch M, Kobbelt L, Pauly M, Alliez P, Lévy B. Polygon Mesh Processing. CRC press; 2010.

[44] Sullivan J. Curvatures of Smooth and Discrete Surfaces. In: Bobenko A, Sullivan J, Schröder P, Ziegler G, editors. Discrete Differential Geometry; Oberwolfach Seminars Vol. 38. Birkhauser Basel; 2008, p. 175–88.

[45] Grinspun E, Gingold Y, Reisman J, Zorin D. Computing Discrete Shape Operators on General Meshes. Computer Graphics Forum (Proc Eurographics) 2006;25(3):547–56.